Observations of Transition from Imbalanced to Balanced Kinetic Alfvénic Turbulence

Jinsong Zhao,[1,*] Trevor A. Bowen,[2] Stuart D. Bale,[3,2] Chen Shi,[4] Thierry Dudok de Wit,[5,6] and Nikos Sioulas[2]

[1]*Purple Mountain Observatory, Chinese Academy of Sciences, Nanjing 210023, People's Republic of China*
[2]*Space Sciences Laboratory, University of California, Berkeley, CA 94720-7450, USA*
[3]*Physics Department, University of California, Berkeley, CA 94720-7300, USA*
[4]*School of Physics and Electronic Sciences, Changsha University of Science and Technology, Changsha, China*
[5]*LPC2E, CNRS, CNES, University of Orléans, Orléans, France*
[6]*International Space Science Institute (ISSI), Bern, Switzerland*

We report observations of solar wind turbulence derived from measurements by the Parker Solar Probe. Our findings reveal the emergence of finite magnetic helicity within the transition range of the turbulence, aligning with signatures of kinetic Alfvén waves (KAWs). Notably, as the wave scale transitions from super-ion to sub-ion scales, the ratio of KAWs with opposing signs of magnetic helicity initially increases from approximately 1 to 6 before returning to 1. This observation provides, for the first time, compelling evidence for the transition from imbalanced kinetic Alfvénic turbulence to balanced kinetic Alfvénic turbulence.

Introduction Alfvénic turbulence is prevalent in the heliosphere [1, 2] and is believed to exist in astrophysical environments [3, 4]. The dissipation of this turbulence is proposed to be a major contributor to heating in the solar wind, solar corona, and other astrophysical plasmas [5–15]. Observations indicate that Alfvénic turbulence encompasses a broad range of scales, evolving from magnetohydrodynamics (MHD) scales down to sub-ion kinetic scales, potentially extending to sub-electron kinetic scales [16–22]. As the turbulence cascade scale approaches the ion gyroradius, anisotropic turbulence models predict a transition from MHD-scale Alfvénic waves to kinetic Alfvén waves (KAWs) [23–30]. Despite substantial evidence of KAWs occurring at ion kinetic scales in satellite observations and numerical simulations [17–22, 31–35], the precise evolution of turbulence at ion kinetic scales remains unknown.

Solar wind turbulence is often highly imbalanced at MHD scales, meaning that outward fluctuations propagating away from the Sun dominate inward fluctuations [1, 36, 37]. Based on the signatures of magnetic helicity at ion scales observed in solar wind turbulence [38–41], it has been suggested that KAWs are predominantly outward-propagating, indicating that imbalanced kinetic Alfvénic turbulence arises at ion kinetic scales [39, 42, 43]. At kinetic scales, imbalanced turbulence may be affected by nonlinear processes from copropagating KAWs or dynamics arising from a helicity barrier [44, 45]. Also, at kinetic scales, the power spectral density of the magnetic field is often characterized by a transition range, occurring at scales approximately equal to the ion gyroradius, and a kinetic-inertial range between ion and electron scales [17–22, 46–48]. These observations prompt a fundamental question concerning the evolution of turbulence at kinetic scales: how does imbalanced Alfvénic turbulence evolve toward smaller scales? This phenomenon remains largely unexplored experimentally.

Using in-situ measurements from Parker Solar Probe [PSP; 49, 50], this Letter investigates solar wind turbulence at kinetic scales. Our findings present, for the first time, observational evidence of the transition from imbalanced to increasingly balanced kinetic Alfvénic turbulence in the solar wind, shedding light on the evolution of imbalanced turbulence.

Methodology Previous studies commonly employ the normalized magnetic helicity, defined as $\sigma_{\rm mTN} = 2{\rm Im}(B_T B_N^*)/B^2$, to identify KAWs, where B_T and B_N represent the magnetic field components in radial-tangential-normal coordinates. It has been suggested that negative (positive) values of $\sigma_{\rm mTN}$ in the outward (inward) sectors of the solar wind magnetic field, particularly as $\theta_{\rm VB} \to 90°$, serve as signatures of KAWs [38, 39, 42, 43, 51]. Here, $\theta_{\rm VB}$ denoting the angle between the solar wind magnetic field $\mathbf{B}$ and the solar wind bulk velocity $\mathbf{V}$. Recently, a novel identification method utilizing magnetic helicity in field-aligned coordinates — based on $\mathbf{B}$ and $\mathbf{V}$ — has been developed to distinguish the signatures of highly oblique KAWs from quasi-parallel ion-scale waves [52]. In this Letter, we enhance this method to analyze kinetic Alfvénic turbulence.

We apply the Morlet wavelet transform to time series magnetic field data merged from fluxgate and search coil magnetometers on PSP/FIELDS [53], with narrowband noise induced by PSP's reaction wheels [54] removed using short-time Fourier transform technology. The data is reconstructed in field-aligned coordinates $(\hat{\mathbf{e}}_{(\mathbf{B_0}\times\mathbf{V_0})\times\mathbf{B_0}}, \hat{\mathbf{e}}_{\mathbf{B_0}\times\mathbf{V_0}}, \hat{\mathbf{e}}_\parallel)$, using averaged values of $\mathbf{B_0}$ and $\mathbf{V_0}$ over 20 seconds. This allow us to obtain the complex wavelet amplitude $\mathbf{W}(f,t)$ at the frequency $f = (w_0 + \sqrt{2+w_0^2})/(4\pi s)$, where the nondimensional frequency $w_0 = 6$ is used [55]. In our definitions, $\hat{\mathbf{e}}_{\mathbf{B_0}\times\mathbf{V_0}} \equiv \mathbf{B_0}\times\mathbf{V_0}/(|\mathbf{B_0}||\mathbf{V_0}|)$, $\hat{\mathbf{e}}_{(\mathbf{B_0}\times\mathbf{V_0})\times\mathbf{B_0}} \equiv \hat{\mathbf{e}}_{\mathbf{B_0}\times\mathbf{V_0}} \times \hat{\mathbf{e}}_\parallel$, and $\hat{\mathbf{e}}_\parallel \equiv \mathbf{B_0}/|\mathbf{B_0}|$. The wavelet scale s is defined accordingly, and the solar wind bulk speed $\mathbf{V}$ is measured by the Solar Probe Cup (SPC) instrument [56] on PSP/SWEAP.

Because KAWs are highly elliptical polarized in the perpendicular direction [57–59], or even appear linearly polarized, we can evaluate their intrinsic perpendicular perturbation components using the two perpendicular components $W_{\mathbf{B_0}\times\mathbf{V_0}}$ and $W_{(\mathbf{B_0}\times\mathbf{V_0})\times\mathbf{B_0}}$. We employ the following procedures. Firstly, we obtain $W_{\perp_1} = W_{\mathbf{B_0}\times\mathbf{V_0}}\cos(\phi) + W_{(\mathbf{B_0}\times\mathbf{V_0})\times\mathbf{B_0}}\sin(\phi)$ and $W_{\perp_2} = -W_{\mathbf{B_0}\times\mathbf{V_0}}\sin(\phi) + W_{(\mathbf{B_0}\times\mathbf{V_0})\times\mathbf{B_0}}\cos(\phi)$ for each sample in (t, f) space in a new perpendicular plane $\hat{\mathbf{e}}_1$–$\hat{\mathbf{e}}_2$, which is defined by rotating the $\hat{\mathbf{e}}_{(\mathbf{B_0}\times\mathbf{V_0})\times\mathbf{B_0}}$ – $\hat{\mathbf{e}}_{\mathbf{B_0}\times\mathbf{V_0}}$ coordinates at an angle ϕ. Then, we determine $W_{\perp_1}$ and $W_{\perp_2}$ by finding maximum $|W_{\perp_2}|$ as ϕ varies between $-\pi/2$ and $\pi/2$. $W_{\perp_2}$ in the new field-aligned coordinates ($\hat{\mathbf{e}}_{\perp_1}$, $\hat{\mathbf{e}}_{\perp_2}$, $\hat{\mathbf{e}}_{\parallel}$) can serve as a reliable indicator of the perpendicular perturbation of KAWs.

Using $W_{\perp_1}$, $W_{\perp_2}$, and $W_{\parallel}$, we define the normalized magnetic helicity as follows:

$$\sigma_{\mathrm{m}\perp_1\perp_2} = -2\mathrm{Im}(W_{\perp_1}W^*_{\perp_2})/|\mathbf{W}|^2, \quad (1)$$

$$\sigma_{\mathrm{m}\perp_2\parallel} = -2\mathrm{Im}(W_{\perp_2}W^*_{\parallel})/|\mathbf{W}|^2, \quad (2)$$

$$\sigma_{\mathrm{m}\parallel\perp_1} = -2\mathrm{Im}(W_{\parallel}W^*_{\perp_1})/|\mathbf{W}|^2, \quad (3)$$

where "$*$" denotes the complex conjugate, and $|\mathbf{W}|^2 = W_{\perp_1}\cdot W^*_{\perp_1} + W_{\perp_2}\cdot W^*_{\perp_2} + W_{\parallel}\cdot W^*_{\parallel}$.

The strong coherence between $W_{\perp_2}$ and $W_{\parallel}$ can result in a non-zero value for $\sigma_{\mathrm{m}\perp_2\parallel}$, indicating the signature of KAWs. Since the coordinates $(\hat{\mathbf{e}}_{\perp_1}, \hat{\mathbf{e}}_{\perp_2}, \hat{\mathbf{e}}_{\parallel})$ are approximately equivalent to the field-aligned coordinates defined by $\left((\hat{\mathbf{e}}_{\parallel}\times\hat{\mathbf{e}}_k)\times\hat{\mathbf{e}}_{\parallel}, \hat{\mathbf{e}}_{\parallel}\times\hat{\mathbf{e}}_k, \hat{\mathbf{e}}_{\parallel}\right)$ (see Supplemental Material [60]), the sign of $\sigma_{\mathrm{m}\perp_2\parallel}$ directly corresponds to the propagation direction of KAWs: a positive value indicates propagation along $\mathbf{B}_0$, while a negative value indicates propagation against $\mathbf{B}_0$. This wave property is consistent between the solar wind frame and the spacecraft frame (see Supplemental Material [60]).

Additionally, the coherent relationship between $W_{\perp_1}$ and $W_{\perp_2}$ can result in a finite value of $\sigma_{\mathrm{m}\perp_1\perp_2}$, which corresponds to the presence of quasi-monochromatic ion cyclotron waves or magnetosonic whistler waves.

Event overview Recent observations from the PSP have revealed a high prevalence of quasi-monochromatic ion-scale waves in the near-Sun solar wind [54, 61–63]. To focus on turbulent fluctuations, we analyze a segment of solar wind data spanning two hours and thirty minutes during Encounter 1, which has a relatively low occurrence rate of these waves. An overview of this typical solar wind is presented in Figure 1.

Figures 1(a) and (b) display the measured magnetic field and solar wind velocity in the spacecraft frame, with $\hat{\mathbf{e}}_z$ oriented sunward. The magnetic field strength remains approximately constant, while its direction shows considerable variability due to the presence of switchbacks. In contrast, the solar wind velocity experiences only minor changes, predominantly streaming outward from the Sun along the radial direction.

Figure 1(c) shows the distribution of $\sigma_{m\perp_1\perp_2}$, which quantifies the polarization of the waves relative to the magnetic field. Positive (red) and negative (blue) values of $\sigma_{m\perp_1\perp_2}$ correspond to right- and left-handed polarized waves, respectively. The data indicate intermittent left-handed polarized waves with $\sigma_{m\perp_1\perp_2} \sim -0.75$ and $f \gtrsim f_{\mathrm{cp}}$, where f and f_{cp} denote the wave frequency and the proton cyclotron frequency, respectively. These polarization characteristics suggest that these waves are left-handed ion-cyclotron waves [54, 61, 62].

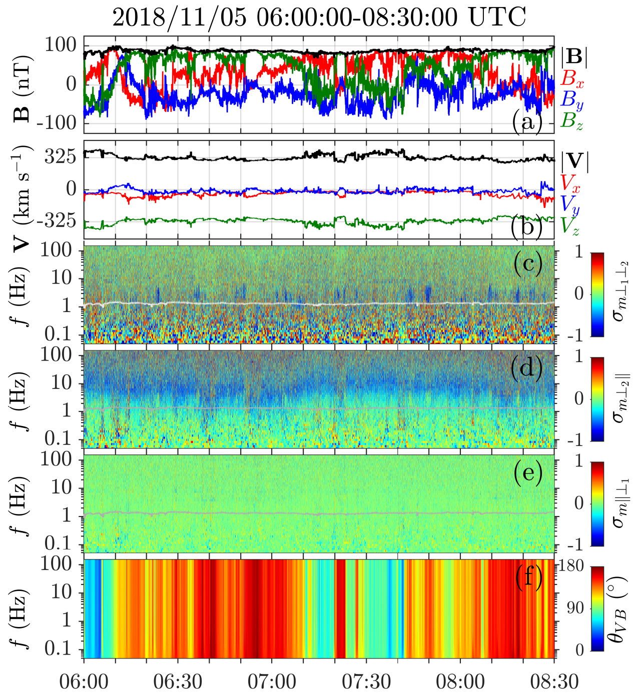

FIG. 1. Plasma environment and magnetic helicity during 06:00-8:30 UTC on 2018 November 5. (a) The strength and three components of the magnetic field $\mathbf{B}$ in the spacecraft frame. (b) The solar wind speed $\mathbf{V}$ in the spacecraft frame. (c) The distribution of $\sigma_{\mathrm{m}\perp_1\perp_2}$. (d) The distribution of $\sigma_{\mathrm{m}\perp_2\parallel}$. (e) The distribution of $\sigma_{\mathrm{m}\parallel\perp_1}$. (f) The distribution of θ_{VB}. The gray curves in (c)–(e) denote the proton cyclotron frequency f_{cp}.

The distribution of $\sigma_{m\perp_2\parallel}$ shown in Figure 1(d) is used to identify KAWs. A clear signature of $\sigma_{m\perp_2\parallel} < 0$ is observed within the frequency range of $f \gtrsim 1$ Hz, indicating the presence of KAWs in the near-Sun solar wind, consistent with previous findings [47, 51]. Furthermore, the signature of negative $\sigma_{m\perp_2\parallel}$ varies over time and is closely linked to the observational features associated with θ_{VB} (Figure 1(f)).

Figure 1(e) illustrates the distribution of $\sigma_{m||\perp_1}$. This quantity typically hovers around zero, suggesting a lack of coherence between $W_{\perp_1}$ and $W_{\parallel}$. Such behavior aligns with theoretical predictions that $\sigma_{m\parallel\perp_1} \sim 0$ for linear KAWs.

Magnetic helicity and turbulent spectra A crucial parameter for analyzing the distribution of magnetic helicity and power spectral density of the magnetic field is θ_{VB}, which represents the angle between the local

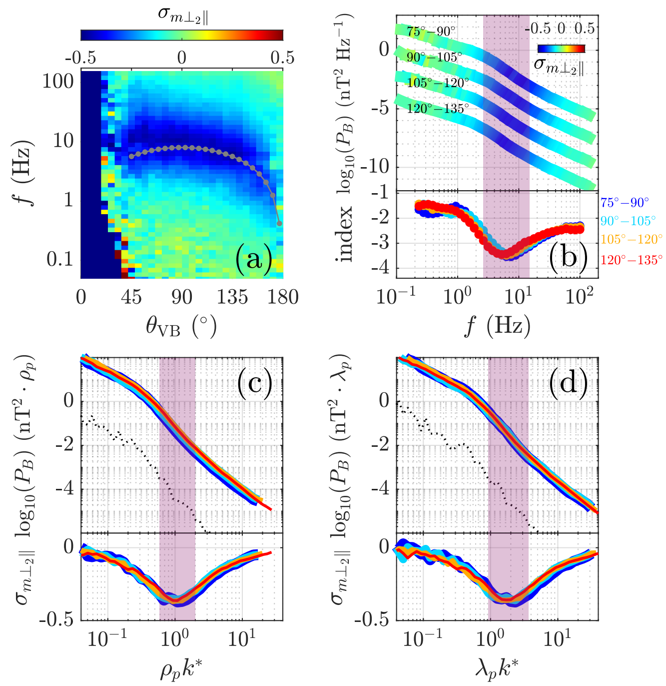

FIG. 2. (a) $\sigma_{m\perp_2\parallel}$ as functions of θ_{VB} and f. Gray points denote the Doppler shifting frequency $f_{\rho_p} = V\sin(\theta_{VB})/(2\pi\rho_p)$ at the averaged proton gyroradius $\rho_p \simeq 6.5$ km. (b) The power spectral density of the magnetic field P_B in four different θ_{VB} ranges: 75°–90°, 90°–105°, 105°–120°, and 120°–135°. The upper panel shows P_B with $\sigma_{m\perp_2\parallel}$ overlaid, whereas the lower panel shows the spectral indices across the four θ_{VB} ranges. (c) P_B (upper panel) and $\sigma_{m\perp_2\parallel}$ (lower panel) as a function of $\rho_p k^*$. (d) P_B (upper panel) and $\sigma_{m\perp_2\parallel}$ (lower panel) as a function of $\lambda_p k^*$. The purple colors in (b)-(d) highlight the transition range. The minimal P_B at each f is used to evaluate the noise level, shown as dotted curves in (c) and (d).

magnetic field direction and the local solar wind velocity direction. This angle is calculated using a Gaussian average [38, 39]. The relationships among these parameters during the selected event are illustrated in Figure 2. To maintain a quiet background for analysis, data with an angular deviation greater than 15° between $\mathbf{B}$ and $\mathbf{B_0}$, referred to as θ_{BB_0}, are excluded from consideration [52].

Figure 2(a) presents the distribution of $\sigma_{m\perp_2\parallel}$ as functions of frequency f and angle θ_{VB}. This figure clearly demonstrates that the observed frequency f increases as θ_{VB} decreases from 180° to 90° for waves exhibiting considerably negative $\sigma_{m\perp_2\parallel}$ (indicated in blue). This trend can be intuitively understood by considering the assumption of quasi-perpendicular waves ($\mathbf{k} \simeq \mathbf{k}_\perp$), which predicts that $f \simeq V_\perp k_\perp/(2\pi)$ in the super-Alfvénic bulk flow, where $V_\perp = V\sin(\theta_{VB})$. The predicted frequency at the proton gyroradius, denoted as $f_{\rho_p} = V_\perp/(2\pi\rho_p)$ (with $\rho_p \sim 6.5$ km), is overlaid in Figure 2(a). The correspondence between the enhanced region of $\sigma_{m\perp_2\parallel} < 0$ and f_{ρ_p} supports the assumption of quasi-perpendicular waves at ion scales.

Figure 2(b) illustrates the power spectral densities of the magnetic field, defined as $P_B(f,\theta_{VB}) = (2dt/N)\sum_i \mathbf{W}(t_i,\theta_{VB}) \cdot \mathbf{W}^*(t_i,\theta_{VB})$, across four θ_{VB} regimes: 75°–90°, 90°–105°, 105°–120°, and 120°–135°. Here, dt represents the time resolution of the magnetic field data, and N is the number of data points in each θ_{VB} range. Assuming that P_B follows a power-law distribution, i.e., $P_B = Cf^\alpha$, we can derive the spectral index α at a specific f by fitting the observed P_B within the frequency range $f/2$ to $2f$. The distribution of α shown in Figure 2(b) reveals a steep transition in the frequency range of approximately 3–15 Hz, where the average value of α is around -3.25 ± 0.05. In contrast, the average α is about -1.62 ± 0.06 in the lower frequency range of approximately 0.2–1 Hz (the inertial range) and -2.52 ± 0.02 in the higher frequency range of approximately 20–100 Hz (the kinetic-inertial range).

To represent P_B in wavenumber space (as discussed by [64]), we employ the expression $P_B(Lk^*,\theta_{VB}) = (dt/\pi N)\sum_i [V_k(t_i)\mathbf{W}(t_i,\theta_{VB}) \cdot \mathbf{W}^*(t_i,\theta_{VB})/L(t_i)]$, where L can be either ρ_p or λ_p (the proton inertial length), $k^* = 2\pi f/V_\perp$, and $V_\perp = V\sin(\theta_{VB})$. Figures 2(c) and (d) illustrate P_B and $\sigma_{m\perp_2\parallel}$ as functions of $\rho_p k^*$ and $\lambda_p k^*$, respectively. Both $P_B(\rho_p k^*)$ and $P_B(\lambda_p k^*)$ exhibit similar power-law distributions across the four θ_{VB} ranges. The transition range occurs at $\rho_p k^* \sim 0.4$–2.2 for $P_B(\rho_p k^*)$ and at $\lambda_p k^* \sim 0.8$–4.2 for $P_B(\lambda_p k^*)$ distributions. This implies that the transition from the inertial to transition range starts at a scale larger than the ion scale, consistent with the prior PSP observations reported by [13].

Transition from imbalanced to balanced kinetic Alfvénic turbulence Because the sign of $\sigma_{m\perp_2\parallel}$ serves as a diagnostic for wave propagation direction, we can elucidate the degree of imbalance in kinetic Alfvénic turbulence by statistically analyzing the number of data points N in the $\sigma_{m\perp_2\parallel}$–$f$ space, as shown in Figure 3.

Figure 3(a) depicts the distribution of $\bar{N}(\sigma_{m\perp_2\parallel}, f)$, which is defined as $N(\sigma_{m\perp_2\parallel}, f)$ normalized by its maximum at each frequency f. The primary features observed are: (1) as f increases, the position of $\bar{N} = 1$ (the maximum N) rapidly shifts to smaller values of $\sigma_{m\perp_2\parallel}$ within $\sim$ 1–10 Hz, mainly arising in the transition range; and (2) $\bar{N}$ in the kinetic-inertial range displays a broader distribution in the $\sigma_{m\perp_2\parallel}$ space compared to that in the transition range.

Figure 3(b) shows the probability distribution function (PDF) of $N(\sigma_{m\perp_2\parallel})$ at four representative frequencies: $f = 0.3$, 3.1, 10.5, and 50.1 Hz. The PDF at $f = 0.3$ Hz roughly follows a Gaussian distribution, suggesting that $\sigma_{m\perp_2\parallel}$ behaves randomly in the inertial range. In the transition range (i.e., at $f = 3.1$ and 10.5 Hz), the PDF exhibits a significant imbalance, indicating that most data points have $\sigma_{m\perp_2\parallel} < 0$. At $f = 50.1$ Hz, the PDF roughly resembles a hat-top distribution, suggesting that turbulence evolves toward a balanced state within the

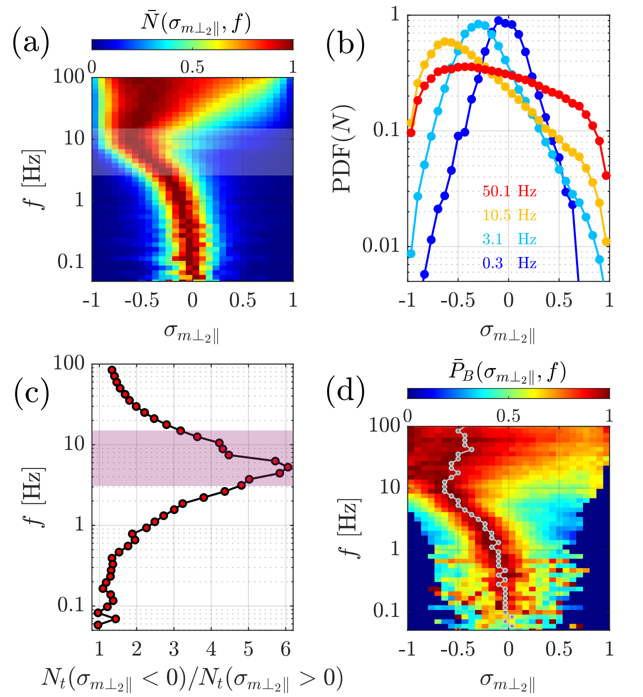

FIG. 3. (a) The number of the data $N(\sigma_{\mathrm{m}\perp_2\parallel}, f)$ normalized by the maximum $N(\sigma_{\mathrm{m}\perp_2\parallel}, f)$ at each f, denoted by $\bar{N}(\sigma_{\mathrm{m}\perp_2\parallel}, f)$. (b) The probability distribution function of $N(\sigma_{\mathrm{m}\perp_2\parallel})$, denoted by PDF($N$), at four typical frequencies: $f = 0.3$, 3.1, 10.5, and 50.1 Hz. (c) The ratio between the total data numbers with negative and positive $\sigma_{\mathrm{m}\perp_2\parallel}$, $N_t(\sigma_{\mathrm{m}\perp_2\parallel} < 0)/N_t(\sigma_{\mathrm{m}\perp_2\parallel} > 0)$. (d) The distribution of P_B normalized by the maximum P_B at each f, where P_B is chosen as the median P_B in the bins in the $\sigma_{\mathrm{m}\perp_2\parallel}$–$f$ space. In (d), the grey curve is the position of $\bar{N} = 1$ in the $\sigma_{\mathrm{m}\perp_2\parallel}$–$f$ space, and the data with number smaller than 1000 are discarded. This figure uses the data limited with $\theta_{\mathrm{BB}_0} < 15°$ and $|\theta_{\mathrm{VB}} - 90°| < 45°$.

kinetic-inertial range.

To quantify the degree of imbalance, we calculate the ratio R of data points with negative to those with positive $\sigma_{\mathrm{m}\perp_2\parallel}$:

$$R = \frac{N_t(\sigma_{\mathrm{m}\perp_2\parallel} < 0)}{N_t(\sigma_{\mathrm{m}\perp_2\parallel} > 0)},$$

as illustrated in Figure 3(c). The value of R initially increases up to $f \sim 5\,\mathrm{Hz}$ before decreasing, indicating a transition from imbalanced to balanced turbulence within the transition range. The frequency $f \sim 5\,\mathrm{Hz}$ corresponds to spatial scales of $\rho_p k \sim 0.6$ and $\lambda_p k \sim 1.3$, which are approximately at the ion characteristic scale.

Finally, Figure 3(d) presents the distribution of P_B as functions of $\sigma_{\mathrm{m}\perp_2\parallel}$ and f, where $P_B(\sigma_{\mathrm{m}\perp_2\parallel}, f)$ is normalized by its maximum value at each frequency f (denoted as $\bar{P}_B$). The position of $\bar{N} = 1$ is overlaid in this figure. We observe that the maximum P_B primarily occurs at $\bar{N} = 1$ between 0.1 and 10 Hz. Above this range, the maximum P_B approximately follows $\bar{N} = 1$ as f. Furthermore, in the kinetic-inertial range, the distribution of $\bar{P}_B$ is broader than that in the transition range, similar to the distribution of $\bar{N}$.

Discussion and conclusions This Letter investigates kinetic Alfvénic turbulence in the near-Sun solar wind, utilizing magnetic field measurements from the PSP. To effectively identify wave modes, we introduce a magnetic helicity method that employs field-aligned coordinates defined by the background magnetic field and the wave vector. Our primary focus is on the magnetic helicity $\sigma_{\mathrm{m}\perp_2\parallel}$, which quantifies the coherence between fluctuations in the parallel magnetic field and principal perpendicular magnetic field fluctuations. This methodology successfully identifies signature of KAWs. Our analysis reveals the prevalence of KAWs characterized by notably negative values of $\sigma_{\mathrm{m}\perp_2\parallel}$, particularly when the wave frequency exceeds the proton cyclotron frequency.

Our examination of the probability density function PDF$(\sigma_{\perp_2\parallel}, f)$ and the ratio $N(\sigma_{\perp_2\parallel} < 0)/N(\sigma_{\perp_2\parallel} > 0)$ reveals two distinct trends as wave frequency increases. First, the PDF$(\sigma_{\perp_2\parallel}, f)$ broadens with respect to $\sigma_{\perp_2\parallel}$. Second, the ratio $N(\sigma_{\perp_2\parallel} < 0)/N(\sigma_{\perp_2\parallel} > 0)$ initially increases before declining. Furthermore, we demonstrate a transition from imbalanced to increasingly balanced kinetic Alfvénic turbulence occurring within the transitional range. Additionally, we find that the wave data number distribution in the $\sigma_{\perp_2\parallel} - f$ space shows a strong correlation with P_B.

These findings prompt two critical questions regarding our understanding of solar wind turbulence at and below the ion scale.

The first question addresses why the imbalance increases toward the transition range. This increase contradicts predictions from models of anisotropic Alfvénic turbulence, which suggest that imbalanced turbulence at the MHD scale evolves toward balance as the turbulent scale decreases [65, 66]. One potential explanation for this contradiction is that the helicity barrier causes a significant portion of the energy flux of outward-propagating waves to become stuck at the ion scale [35, 45], resulting in an increase in imbalance. Additionally, there may be another source of KAWs beyond the anisotropic cascade and helicity barrier models. Although previous studies have suggested that plasma instabilities can generate KAWs [67, 68], observational evidence supporting this claim remains limited.

The second question addresses the evolution of turbulence within the kinetic-inertial range. Our observations reveal that turbulence in this range remains imbalanced, with outward KAWs carrying a larger portion of the wave energy compared to inward KAWs. This finding contrasts with the predictions of the helicity barrier turbulence model [35], which suggests the formation of balanced turbulence. Thus, a definitive resolution to this discrepancy remains unclear.

In conclusion, the novel observations presented in this Letter highlight the necessity for new theoretical frameworks to accurately model solar wind turbulence at kinetic scales.

This study is supported by the Strategic Priority Research Program of the Chinese Academy of Sciences (Grant No. XDB0560000) and the National Key R&D Program of China 2022YFF0503000 (2022YFF0503003). Z.J.S. thanks for the support from NSFC 42374196. TDdW acknowledges support from CNES. The FIELDS and SWEAP instruments were designed and built under NASA Contract No. NNN06AA01C.

* zhaojs82@gmail.com

[1] C. Y. Tu and E. Marsch, Magnetohydrodynamic Structures Waves and Turbulence in the Solar Wind - Observations and Theories, Space Science Reviews **73**, 1 (1995).

[2] R. Bruno and V. Carbone, The Solar Wind as a Turbulence Laboratory, Living Reviews in Solar Physics **2**, 4 (2005).

[3] J. W. Armstrong, B. J. Rickett, and S. R. Spangler, Electron Density Power Spectrum in the Local Interstellar Medium, Astrophysical Journal **443**, 209 (1995).

[4] P. Goldreich and S. Sridhar, Toward a Theory of Interstellar Turbulence. II. Strong Alfvenic Turbulence, Astrophysical Journal **438**, 763 (1995).

[5] E. Quataert and A. Gruzinov, Turbulence and Particle Heating in Advection-dominated Accretion Flows, The Astrophysical Journal **520**, 248 (1999).

[6] C. W. Smith, K. Hamilton, B. J. Vasquez, and R. J. Leamon, Dependence of the Dissipation Range Spectrum of Interplanetary Magnetic Fluctuationson the Rate of Energy Cascade, The Astrophysical Journal Letters **645**, L85 (2006).

[7] S. R. Cranmer, A. A. van Ballegooijen, and R. J. Edgar, Self-consistent Coronal Heating and Solar Wind Acceleration from Anisotropic Magnetohydrodynamic Turbulence, The Astrophysical Journal Supplement Series **171**, 520 (2007).

[8] A. A. van Ballegooijen, M. Asgari-Targhi, S. R. Cranmer, and E. E. DeLuca, Heating of the Solar Chromosphere and Corona by Alfvén Wave Turbulence, The Astrophysical Journal.

[9] B. D. G. Chandran, B. Li, B. N. Rogers, E. Quataert, and K. Germaschewski, Perpendicular Ion Heating by Low-frequency Alfvén-wave Turbulence in the Solar Wind, The Astrophysical Journal **720**, 503 (2010).

[10] B. D. G. Chandran, Alfvén-wave Turbulence and Perpendicular Ion Temperatures in Coronal Holes, The Astrophysical Journal **720**, 548 (2010).

[11] Y. Kawazura, M. Barnes, and A. A. Schekochihin, Thermal Disequilibration of Ions and Electrons by Collisionless Plasma Turbulence, Proceedings of the National Academy of Science **116**, 771 (2019).

[12] L. Arzamasskiy, M. W. Kunz, B. D. G. Chandran, and E. Quataert, Hybrid-kinetic Simulations of Ion Heating in Alfvénic Turbulence, The Astrophysical Journal **879**, 53 (2019).

[13] T. A. Bowen, A. Mallet, S. D. Bale, J. W. Bonnell, A. W. Case, B. D. G. Chandran, A. Chasapis, C. H. K. Chen, D. Duan, T. Dudok de Wit, K. Goetz, J. S. Halekas, P. R. Harvey, J. C. Kasper, K. E. Korreck, D. Larson, R. Livi, R. J. MacDowall, D. M. Malaspina, M. D. McManus, M. Pulupa, M. Stevens, and P. Whittlesey, Constraining Ion-Scale Heating and Spectral Energy Transfer in Observations of Plasma Turbulence, Physical Review Letters **125**, 025102 (2020).

[14] H. Wu, C. Tu, X. Wang, J. He, and L. Yang, Energy Supply for Heating the Slow Solar Wind Observed by Parker Solar Probe between 0.17 and 0.7 au, The Astrophysical Journal Letters **904**, L8 (2020).

[15] H. Wu, C. Tu, X. Wang, J. He, L. Yang, and S. Yao, Energy Supply by Low-frequency Break Sweeping for Heating the Fast Solar Wind from 0.3 to 4.8 au, The Astrophysical Journal **912**, 84 (2021).

[16] R. J. Leamon, C. W. Smith, N. F. Ness, W. H. Matthaeus, and H. K. Wong, Observational Constraints on the Dynamics of the Interplanetary Magnetic Field Dissipation Range, Journal of Geophysical Research: Space Physics **103**, 4775 (1998).

[17] S. D. Bale, P. J. Kellogg, F. S. Mozer, T. S. Horbury, and H. Reme, Measurement of the Electric Fluctuation Spectrum of Magnetohydrodynamic Turbulence, Physical Review Letters **94**, 215002 (2005).

[18] O. Alexandrova, J. Saur, C. Lacombe, A. Mangeney, J. Mitchell, S. J. Schwartz, and P. Robert, Universality of Solar-Wind Turbulent Spectrum from MHD to Electron Scales, Physical Review Letters **103**, 165003 (2009).

[19] F. Sahraoui, M. L. Goldstein, P. Robert, and Y. V. Khotyaintsev, Evidence of a Cascade and Dissipation of Solar-Wind Turbulence at the Electron Gyroscale, Physical Review Letters **102**, 231102 (2009).

[20] F. Sahraoui, M. L. Goldstein, G. Belmont, P. Canu, and L. Rezeau, Three Dimensional Anisotropic k Spectra of Turbulence at Subproton Scales in the Solar Wind, Physical Review Letters **105**, 131101 (2010).

[21] C. S. Salem, G. G. Howes, D. Sundkvist, S. D. Bale, C. C. Chaston, C. H. K. Chen, and F. S. Mozer, Identification of Kinetic Alfvén Wave Turbulence in the Solar Wind, The Astrophysical Journal Letters **745**, L9 (2012).

[22] C. H. K. Chen, S. Boldyrev, Q. Xia, and J. C. Perez, Nature of Subproton Scale Turbulence in the Solar Wind, Physical Review Letters **110**, 225002 (2013).

[23] E. Quataert, Particle Heating by Alfvénic Turbulence in Hot Accretion Flows, The Astrophysical Journal **500**, 978 (1998).

[24] G. G. Howes, S. C. Cowley, W. Dorland, G. W. Hammett, E. Quataert, and A. A. Schekochihin, A Model of Turbulence in Magnetized Plasmas: Implications for the Dissipation Range in the Solar Wind, Journal of Geophysical Research: Space Physics **113**, A05103 (2008).

[25] A. A. Schekochihin, S. C. Cowley, W. Dorland, G. W. Hammett, G. G. Howes, E. Quataert, and T. Tatsuno, Astrophysical Gyrokinetics: Kinetic and Fluid Turbulent Cascades in Magnetized Weakly Collisional Plasmas, The Astrophysical Journal Supplement Series **182**, 310 (2009).

[26] Y. Voitenko and J. de Keyser, Turbulent Spectra and Spectral Kinks in the Transition Range from MHD to Kinetic Alfvén Turbulence, Nonlinear Processes in Geophysics **18**, 587 (2011).

[27] S. Boldyrev and J. C. Perez, Spectrum of Kinetic-Alfvén Turbulence, The Astrophysical Journal Letters **758**, L44

(2012).
[28] J. S. Zhao, D. J. Wu, and J. Y. Lu, Kinetic Alfvén Turbulence and Parallel Electric Fields in Flare Loops, The Astrophysical Journal **767**, 109 (2013).
[29] J. S. Zhao, Y. M. Voitenko, D. J. Wu, and M. Y. Yu, Kinetic Alfvén Turbulence Below and Above Ion Cyclotron Frequency, Journal of Geophysical Research: Space Physics **121**, 5 (2016).
[30] C. H. K. Chen and S. Boldyrev, Nature of Kinetic Scale Turbulence in the Earth's Magnetosheath, The Astrophysical Journal **842**, 122 (2017).
[31] G. G. Howes, J. M. Tenbarge, W. Dorland, E. Quataert, A. A. Schekochihin, R. Numata, and T. Tatsuno, Gyrokinetic Simulations of Solar Wind Turbulence from Ion to Electron Scales, Physical Review Letters **107**, 035004 (2011).
[32] L. Franci, S. Landi, L. Matteini, A. Verdini, and P. Hellinger, High-resolution Hybrid Simulations of Kinetic Plasma Turbulence at Proton Scales, The Astrophysical Journal **812**, 21 (2015).
[33] D. Grošelj, A. Mallet, N. F. Loureiro, and F. Jenko, Fully Kinetic Simulation of 3D Kinetic Alfvén Turbulence, Physical Review Letters **120**, 105101 (2018).
[34] D. Grošelj, C. H. K. Chen, A. Mallet, R. Samtaney, K. Schneider, and F. Jenko, Kinetic Turbulence in Astrophysical Plasmas: Waves and/or Structures?, Physical Review X **9**, 031037 (2019).
[35] J. Squire, R. Meyrand, M. W. Kunz, L. Arzamasskiy, A. A. Schekochihin, and E. Quataert, High-frequency Heating of the Solar Wind Triggered by Low-frequency Turbulence, Nature Astronomy **6**, 715 (2022).
[36] C. H. K. Chen, S. D. Bale, C. S. Salem, and B. A. Maruca, Residual Energy Spectrum of Solar Wind Turbulence, The Astrophysical Journal **770**, 125 (2013).
[37] L. Yang, J. He, D. Verscharen, H. Li, T. A. Bowen, S. D. Bale, H. Wu, W. Li, Y. Wang, L. Zhang, X. Feng, and Z. Wu, Energy Transfer of Imbalanced Alfvénic Turbulence in the Heliosphere, Nature Communications **14**, 7955 (2023).
[38] J. He, E. Marsch, C. Tu, S. Yao, and H. Tian, Possible Evidence of Alfvén-cyclotron Waves in the Angle Distribution of Magnetic Helicity of Solar Wind Turbulence, The Astrophysical Journal **731**, 85 (2011).
[39] J. J. Podesta and S. P. Gary, Magnetic Helicity Spectrum of Solar Wind Fluctuations as a Function of the Angle with Respect to the Local Mean Magnetic Field, The Astrophysical Journal **734**, 15 (2011).
[40] D. Telloni, R. Bruno, and L. Trenchi, Radial Evolution of Spectral Characteristics of Magnetic Field Fluctuations at Proton Scales, Astrophys. J. **805**, 46 (2015).
[41] D. Telloni, R. Bruno, R. D'Amicis, F. Carbone, R. De Marco, and D. Perrone, Wave-polarization Analysis of the Alfvénic Slow Solar Wind at Kinetic Scales, Astrophys. J. **897**, 167 (2020).
[42] J. He, C. Tu, E. Marsch, and S. Yao, Reproduction of the Observed Two-component Magnetic Helicity in Solar Wind Turbulence by a Superposition of Parallel and Oblique Alfvén Waves, The Astrophysical Journal **749**, 86 (2012).
[43] K. G. Klein, G. G. Howes, J. M. TenBarge, and J. J. Podesta, Physical Interpretation of the Angle-dependent Magnetic Helicity Spectrum in the Solar Wind: The Nature of Turbulent Fluctuations near the Proton Gyroradius Scale, The Astrophysical Journal **785**, 138 (2014).
[44] Y. Voitenko and J. De Keyser, MHD-Kinetic Transition in Imbalanced Alfvénic Turbulence, The Astrophysical Journal Letters **832**, L20 (2016).
[45] R. Meyrand, J. Squire, A. A. Schekochihin, and W. Dorland, On the Violation of the Zeroth Law of Turbulence in Space Plasmas, Journal of Plasma Physics **87**, 535870301 (2021).
[46] D. Duan, T. A. Bowen, C. H. K. Chen, A. Mallet, J. He, S. D. Bale, D. Vech, J. C. Kasper, M. Pulupa, J. W. Bonnell, A. W. Case, T. D. de Wit, K. Goetz, P. R. Harvey, K. E. Korreck, D. Larson, R. Livi, R. J. MacDowall, D. M. Malaspina, M. Stevens, and P. Whittlesey, The Radial Dependence of Proton-scale Magnetic Spectral Break in Slow Solar Wind during PSP Encounter 2, The Astrophysical Journal Supplement Series **246**, 55 (2020).
[47] D. Duan, J. He, T. A. Bowen, L. D. Woodham, T. Wang, C. H. K. Chen, A. Mallet, and S. D. Bale, Anisotropy of Solar Wind Turbulence in the Inner Heliosphere at Kinetic Scales: PSP Observations, The Astrophysical Journal Letters **915**, L8 (2021).
[48] S. Y. Huang, F. Sahraoui, N. Andrés, L. Z. Hadid, Z. G. Yuan, J. S. He, J. S. Zhao, S. Galtier, J. Zhang, X. H. Deng, K. Jiang, L. Yu, S. B. Xu, Q. Y. Xiong, Y. Y. Wei, T. Dudok de Wit, S. D. Bale, and J. C. Kasper, The Ion Transition Range of Solar Wind Turbulence in the Inner Heliosphere: Parker Solar Probe Observations, The Astrophysical Journal Letters **909**, L7 (2021).
[49] S. D. Bale, K. Goetz, P. R. Harvey, P. Turin, J. W. Bonnell, T. Dudok de Wit, R. E. Ergun, R. J. MacDowall, M. Pulupa, M. Andre, M. Bolton, J. L. Bougeret, T. A. Bowen, D. Burgess, C. A. Cattell, B. D. G. Chandran, C. C. Chaston, C. H. K. Chen, M. K. Choi, J. E. Connerney, S. Cranmer, M. Diaz-Aguado, W. Donakowski, J. F. Drake, W. M. Farrell, P. Fergeau, J. Fermin, J. Fischer, N. Fox, D. Glaser, M. Goldstein, D. Gordon, E. Hanson, S. E. Harris, L. M. Hayes, J. J. Hinze, J. V. Hollweg, T. S. Horbury, R. A. Howard, V. Hoxie, G. Jannet, M. Karlsson, J. C. Kasper, P. J. Kellogg, M. Kien, J. A. Klimchuk, V. V. Krasnoselskikh, S. Krucker, J. J. Lynch, M. Maksimovic, D. M. Malaspina, S. Marker, P. Martin, J. Martinez-Oliveros, J. McCauley, D. J. McComas, T. McDonald, N. Meyer-Vernet, M. Moncuquet, S. J. Monson, F. S. Mozer, S. D. Murphy, J. Odom, R. Oliverson, J. Olson, E. N. Parker, D. Pankow, T. Phan, E. Quataert, T. Quinn, S. W. Ruplin, C. Salem, D. Seitz, D. A. Sheppard, A. Siy, K. Stevens, D. Summers, A. Szabo, M. Timofeeva, A. Vaivads, M. Velli, A. Yehle, D. Werthimer, and J. R. Wygant, The FIELDS Instrument Suite for Solar Probe Plus. Measuring the Coronal Plasma and Magnetic Field, Plasma Waves and Turbulence, and Radio Signatures of Solar Transients, Space Science Reviews **204**, 49 (2016).
[50] J. C. Kasper, R. Abiad, G. Austin, M. Balat-Pichelin, S. D. Bale, J. W. Belcher, P. Berg, H. Bergner, M. Berthomier, J. Bookbinder, E. Brodu, D. Caldwell, A. W. Case, B. D. G. Chandran, P. Cheimets, J. W. Cirtain, S. R. Cranmer, D. W. Curtis, P. Daigneau, G. Dalton, B. Dasgupta, D. DeTomaso, M. Diaz-Aguado, B. Djordjevic, B. Donaskowski, M. Effinger, V. Florinski, N. Fox, M. Freeman, D. Gallagher, S. P. Gary, T. Gauron, R. Gates, M. Goldstein, L. Golub, D. A. Gordon, R. Gurnee, G. Guth, J. Halekas, K. Hatch, J. Heerikuisen, G. Ho, Q. Hu, G. Johnson, S. P. Jor-

dan, K. E. Korreck, D. Larson, A. J. Lazarus, G. Li, R. Livi, M. Ludlam, M. Maksimovic, J. P. McFadden, W. Marchant, B. A. Maruca, D. J. McComas, L. Messina, T. Mercer, S. Park, A. M. Peddie, N. Pogorelov, M. J. Reinhart, J. D. Richardson, M. Robinson, I. Rosen, R. M. Skoug, A. Slagle, J. T. Steinberg, M. L. Stevens, A. Szabo, E. R. Taylor, C. Tiu, P. Turin, M. Velli, G. Webb, P. Whittlesey, K. Wright, S. T. Wu, and G. Zank, Solar Wind Electrons Alphas and Protons (SWEAP) Investigation: Design of the Solar Wind and Coronal Plasma Instrument Suite for Solar Probe Plus, Space Science Reviews **204**, 131 (2016).

[51] S. Y. Huang, J. Zhang, F. Sahraoui, J. S. He, Z. G. Yuan, N. Andrés, L. Z. Hadid, X. H. Deng, K. Jiang, L. Yu, Q. Y. Xiong, Y. Y. Wei, S. B. Xu, S. D. Bale, and J. C. Kasper, Kinetic Scale Slow Solar Wind Turbulence in the Inner Heliosphere: Coexistence of Kinetic Alfvén Waves and Alfvén Ion Cyclotron Waves, The Astrophysical Journal Letters **897**, L3 (2020).

[52] L. D. Woodham, R. T. Wicks, D. Verscharen, J. M. TenBarge, and G. G. Howes, Dependence of Solar Wind Proton Temperature on the Polarization Properties of Alfvénic Fluctuations at Ion-kinetic Scales, The Astrophysical Journal **912**, 101 (2021).

[53] T. A. Bowen, S. D. Bale, J. W. Bonnell, T. Dudok de Wit, K. Goetz, K. Goodrich, J. Gruesbeck, P. R. Harvey, G. Jannet, A. Koval, R. J. MacDowall, D. M. Malaspina, M. Pulupa, C. Revillet, D. Sheppard, and A. Szabo, A Merged Search-Coil and Fluxgate Magnetometer Data Product for Parker Solar Probe FIELDS, Journal of Geophysical Research: Space Physics **125**, e27813 (2020).

[54] T. A. Bowen, A. Mallet, J. Huang, K. G. Klein, D. M. Malaspina, M. Stevens, S. D. Bale, J. W. Bonnell, A. W. Case, B. D. G. Chandran, C. C. Chaston, C. H. K. Chen, T. Dudok de Wit, K. Goetz, P. R. Harvey, G. G. Howes, J. C. Kasper, K. E. Korreck, D. Larson, R. Livi, R. J. MacDowall, M. D. McManus, M. Pulupa, J. L. Verniero, and P. Whittlesey, Ion-scale Electromagnetic Waves in the Inner Heliosphere, The Astrophysical Journal Supplement Series **246**, 66 (2020).

[55] C. Torrence and G. P. Compo, A Practical Guide to Wavelet Analysis., Bulletin of the American Meteorological Society **79**, 61 (1998).

[56] A. W. Case, J. C. Kasper, M. L. Stevens, K. E. Korreck, K. Paulson, P. Daigneau, D. Caldwell, M. Freeman, T. Henry, B. Klingensmith, J. A. Bookbinder, M. Robinson, P. Berg, C. Tiu, J. Wright, K. H., M. J. Reinhart, D. Curtis, M. Ludlam, D. Larson, P. Whittlesey, R. Livi, K. G. Klein, and M. M. Martinović, The Solar Probe Cup on the Parker Solar Probe, The Astrophysical Journal Supplement Series **246**, 43 (2020).

[57] J. V. Hollweg, Kinetic Alfvén Wave Revisited, Journal of Geophysical Research **104**, 14811 (1999).

[58] J. S. Zhao, Y. Voitenko, M. Y. Yu, J. Y. Lu, and D. J. Wu, Properties of Short-wavelength Oblique Alfvén and Slow Waves, Astrophys. J. **793**, 107 (2014).

[59] J. Zhao, L. Lee, H. Xie, Y. Yao, D. Wu, Y. Voitenko, and V. Pierrard, Quantifying Wave-Particle Interactions in Collisionless Plasmas: Theory and Its Application to the Alfvén-mode Wave, Astrophys. J. **930**, 95 (2022).

[60] See Supplemental Material at [URL will be inserted by publisher] for a description of the field-aligned coordinates and the theoretical predictions of the wave properties of KAWs, which include Refs. [58, 69].

[61] J. L. Verniero, D. E. Larson, R. Livi, A. Rahmati, M. D. McManus, P. S. Pyakurel, K. G. Klein, T. A. Bowen, J. W. Bonnell, B. L. Alterman, P. L. Whittlesey, D. M. Malaspina, S. D. Bale, J. C. Kasper, A. W. Case, K. Goetz, P. R. Harvey, K. E. Korreck, R. J. MacDowall, M. Pulupa, M. L. Stevens, and T. D. de Wit, Parker Solar Probe Observations of Proton Beams Simultaneous with Ion-scale Waves, The Astrophysical Journal Supplement Series **248**, 5 (2020).

[62] W. Liu, J. Zhao, T. Wang, X. Dong, J. C. Kasper, S. D. Bale, C. Shi, and D. Wu, The Radial Distribution of Ion-scale Waves in the Inner Heliosphere, The Astrophysical Journal **951**, 69 (2023).

[63] C. Shi, J. Zhao, S. Liu, F. Xiao, Y. Wu, T. A. Bowen, R. Livi, and S. D. Bale, Coexistence of Antisunward and Sunward Ion Cyclotron Waves in the Near-Sun Solar Wind: Excitation by the Proton Cyclotron Instability, The Astrophysical Journal Letter **971**, L41 (2024).

[64] N. Sioulas, Z. Huang, C. Shi, M. Velli, A. Tenerani, T. A. Bowen, S. D. Bale, J. Huang, L. Vlahos, L. D. Woodham, T. S. Horbury, T. D. de Wit, D. Larson, J. Kasper, C. J. Owen, M. L. Stevens, A. Case, M. Pulupa, D. M. Malaspina, J. W. Bonnell, R. Livi, K. Goetz, P. R. Harvey, R. J. MacDowall, M. Maksimović, P. Louarn, and A. Fedorov, Magnetic Field Spectral Evolution in the Inner Heliosphere, The Astrophysical Journal Letters **943**, L8 (2023).

[65] B. D. G. Chandran, Strong Anisotropic MHD Turbulence with Cross Helicity, Astrophys. J. **685**, 646 (2008).

[66] A. A. Schekochihin, MHD Turbulence: A Biased Review, Journal of Plasma Physics **88**, 155880501 (2022).

[67] O. Alexandrova, C. H. K. Chen, L. Sorriso-Valvo, T. S. Horbury, and S. D. Bale, Solar Wind Turbulence and the Role of Ion Instabilities, Space Science Reviews **178**, 101 (2013).

[68] P. Hellinger, L. Matteini, S. Landi, A. Verdini, L. Franci, and P. M. Trávníček, Plasma Turbulence and Kinetic Instabilities at Ion Scales in the Expanding Solar Wind, The Astrophysical Journal Letters **811**, L32 (2015).

[69] S. P. Gary, Low-frequency Waves In a High-beta Collisionless Plasma: Polarization, Compressibility and Helicity, Journal of Plasma Physics **35**, 431 (1986).